SPE-211691-MS

Automated Image Processing of Petrographic Thin Sections for Digital Reservoir Description: A Bridge to Correlate with Core and NMR Data

Rathnakar Reddy Peesu, Deepak Kumar Voleti, Ashim Dutta, Prabhakar Reddy Vanam, and Nagaraju Reddicharla, ADNOC Onshore

Copyright 2022, Society of Petroleum Engineers DOI 10.2118/211691-MS

This paper was prepared for presentation at the ADIPEC held in Abu Dhabi, UAE, 31 October – 3 November 2022.

This paper was selected for presentation by an SPE program committee following review of information contained in an abstract submitted by the author(s). Contents of the paper have not been reviewed by the Society of Petroleum Engineers and are subject to correction by the author(s). The material does not necessarily reflect any position of the Society of Petroleum Engineers, its officers, or members. Electronic reproduction, distribution, or storage of any part of this paper without the written consent of the Society of Petroleum Engineers is prohibited. Permission to reproduce in print is restricted to an abstract of not more than 300 words; illustrations may not be copied. The abstract must contain conspicuous acknowledgment of SPE copyright.

Abstract

Carbonates exhibits diverse flow characteristics at pore scale. Petrographic study reveals micro-level heterogeneities. Thin sections are key to assess reservoir quality although these are images and interpretations in text format. Thin section microscopic analysis is descriptive and subjective. To an extent, optical point counting is routinely used quantitatively to estimate porosity, cement, and granular features. Overall, thin section descriptions require specialist human skill and an extensive effort, as it is repetitive and time consuming. Thus, a manual process limits the overall progress of rock quality assessment. There is no recognized method to handle thin sections for direct input with conventional core data due to its image and descriptive nature of data. An automated image processing is one of the emerging concepts designed in this paper to batch process thin sections for digital reservoir descriptions and cross correlating the results with conventional core analysis data.

Thin section images are photomicrographs under plane polarized light. Initially, denoise and image enhancement techniques were implemented to preserve elemental boundaries. Computational algorithms mainly, multilevel thresholding and pixel intensity clustering algorithms were programmed to segment images for extracting elements from segmented regions. The extracted elements were compared with original image for labeling. The labeled elements are interpreted for geological elements such as matrix, pores, cement, and other granular content. The interpreted geological elements are then measured for their physical properties like area, equivalent diameter, perimeter, solidity, eccentricity, and entropy. 2D-Porosity, polymodal pore size distribution, mean pore size, cement and granular contents were then derived for each thin section image. The estimated properties were compared with conventional core after calibrating with laboratory NMR data. The whole process is automated in a batch process for a specific reservoir type and computational cost is analyzed for optimization.

2D-porosity is in excellent agreement with core porosity, thus reducing uncertainty that arises from visual estimations. Scale related issues were highlighted between 2D porosity and core porosity for some samples. Polymodal pore size distributions are in good correlation with NMR T2 distribution compared to MICP distributions. The correlation coefficient was understood to be equivalent to surface relaxivity. A digital dataset consisting of 2D porosity, eccentricity, entropy, mean pore size, cement and grain contents

Downloaded from http://onepetro.org/SPEADIP/proceedings-pdf/22ADIP/1-22ADIP/D012S145R004/3045811/spe-211691-ms.pdf by China University of Petroleum (East China) user on 08 July 2023

is automatically extracted in csv format. The digital dataset, which was previously in text format in conventional analysis, is now a rich quantitative dataset.

This paper demonstrated a unique and customized solution to extract digital reservoir descriptions for geoscience applications. This significantly reduced the subjectivity in visual descriptions. The solution presented is scalable to large number of samples with significant reduction in turnaround and effort compared to conventional techniques. Additional merit is that the result from this method has direct correlation to conventional core data for improving rock typing workflows. This paper presents a novel means to use thin section images directly in digital format in geoscience applications.

Introduction

Carbonate reservoirs are heterogenous and exhibit diverse flow characteristics at pore scale. Petrographic thin section study provides geological constituents, pore characteristics and micro-level heterogeneities. Conventional thin section microscopic analysis is descriptive and subjective. Optical point counting (Delesse 1848; Chayes 1949) is a routine technique for quantitative thin section description. Optical counting requires thin section sample grounded to 30 microns at which thickness the sample is transparent for light. Performing optical point counting is a cumbersome process with domain expert making observations at various positions by moving microscope on thin section. Optical point counting provides data for modal analysis to further augment thin section descriptions. Image processing methods are evolved as an alternative to optical point counting methods alleviating the challenges such as navigability of microscope at various grid sections, selection of grid size and domain expertise for accurate observations. Petrographic image analysis (PIA) is one of the image processing methods carried out to derive pore types by analyzing thin section images. Petrographic image analysis (PIA) is widely discussed in literature (Ehrlich and Korkowitz 1987; Ehrlich et al. 1991a). PIA involves estimation of two-dimensional(2-D) geometric parameters of pore network crosssection for deriving three-dimensional(3-D) petrophysical properties. Key results from PIA includes pore size, shape, frequency, and total porosity. PIA is an effective method for reservoir evaluation when there exists an established correlation between 2-D geometric parameters measured on thin section to 3-D petrophysical properties on cores. Several authors (Gerard et al. 1992; Gies 1993; Carr et al. 1995) in the past had attempted successfully to integrate two-dimensional(2-D) reservoir properties from thin section with 3-D petrophysical properties. The integration of 2-D geometric properties with 3-D petrophysical properties at plug scale is not straight forward without honoring complex pore types present in reservoirs i.e., carbonates. There is no recognized method in this regard to demonstrate the bridge between the 2-D geometric properties from thin sections and conventional core analysis data at plug scale.

Bowers et al. (1995) proposed a procedure for calibration between NMR derived poretypes and image derived poretypes. Carr et al. (1995) also conducted similar procedure for carbonate reservoirs. Both procedures (i.e., Bowers et al. (1995); and Carr et al. (1995)) used NMR longitudinal relaxation time(T1) for NMR pore types for cross validating with image derived pore types. The common result from these methods is deriving a value for surface relaxivity(ρ) relating NMR T1 and pore size distributions. Measuring full cycle of NMR T1 distributions is not possible at practical logging speeds in wells. NMR transverse relaxation time(T2) distributions also exhibit pore size distributions when measured on water saturated core plugs. The dominant relaxation process is surface relaxation as bulk relaxation and diffusion effects are minimal under water saturation conditions. T2 distributions are routinely measured in the laboratory and are also acquired as part of logging programs. Therefore, calibration of image derived pore types to NMR T2 distributions offer the necessary bridge between 2D reservoir properties and 3D reservoir properties in core/log domain. Digital Image processing is also improved over years with the emergence of machinal learning and artificial intelligence in computer vision processing.

Downloaded from http://onepetro.org/SPEADIP/proceedings-pdf/22ADIP/1-22ADIP/D012S145R004/3045811/spe-211691-ms.pdf by China University of Petroleum (East China) user on 08 July 2023

The work presented in this paper leverages the modern image segmentation techniques namely multilevel thresholding (Chen and Chung 2001), pixel intensity clustering (Olugbara et al. 2015), and computing power. Algorithms are customized for thin section image processing by honoring complex pore types in carbonate reservoirs. Integration of laboratory nuclear magnetic resonance (NMR) data enabled the bridge required for the integration of 2-D geometric properties with conventional core analysis data. The computational cost is optimized while automating. Batch processing of multiple thin sections paved the way for digital reservoir description in a swift turnaround time.

Statement of Purpose

Thin section images are photomicrographs of thin section samples with vacuum impregnated by blue-dyed epoxy resin. Domain expert conducts petrographic study on photomicrographs under microscope for detailed thin section description. Although the process is time consuming and repetitive, it is subjective at times. Thin section studies are conducted on cores acquired at various times during reservoir development. The results of thin section study are in text format with annotation on thin section images (**Figure 1**). Data format of the results from thin section studies are not readily compatible with conventional core analysis data for direct input to geoscience applications in rock typing studies. Thin section descriptions should be consistent, quantifiable, and cross-correlated to conventional core analysis data for a robust reservoir characterization. Carbonate reservoirs undergo multiple paragenetic sequences developing complex pore types. Thin section descriptions are the source to understand diagenetic events causing either destruction or enhancement of porosity in carbonate reservoirs. Evolution of computer vision processing proved to be a potential alternative to microscopic aided thin section descriptions. However, image processing for digital thin section descriptions involves using two-dimensional (2D) geometrical parameters to derive three-dimensional reservoir properties. Fundamental assumption here is from Delesse's principle (Weibel 1979) which states that volume density of various components making up a rock can be estimated on random sections by measuring areal density of various profiles on those sections. In other words, three-dimensional information can be extracted from high quality and representative two-dimensional data. However, implementation of digital image processing methods on thin sections is challenged due to heterogenous nature of carbonate reservoirs. There is no recognized method to calibrate two-dimensional properties from thin section to conventional core analysis data honoring inherent heterogeneity present in carbonate reservoirs.

The objective of proposed methodology is as follow

- Digital reservoir description of petrographic thin sections instead of text and image formats to correlate with conventional core analysis data at plug scale
- Cross-validated digital reservoir properties from thin section depicting and honoring inherent reservoir heterogeneity

Downloaded from http://onepetro.org/SPEADIP/proceedings-pdf/22ADIP/1-22ADIP/D012S145R004/3045811/spe-211691-ms.pdf by China University of Petroleum (East China) user on 08 July 2023

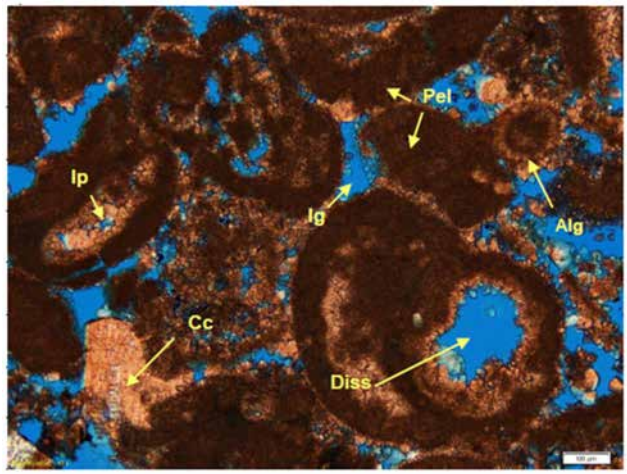

Figure 1—Annotated thin section microphotograph from a carbonate reservoir (Cc: Calcite cementation, Diss: dissolution; Ig: Intergranular porosity; Ip: Intra skeletal porosity; Pel: Peloidal grains; Alg: Micritic matrix)

Theoretical Overview

Image segmentation is the cornerstone of all image processing methods. Segmented image is used for estimating geometric parameters of constituents present in the image. Two algorithms are considered in the proposed workflow namely a fast algorithm for multilevel thresholding and pixel intensity clustering algorithm for multilevel image segmentation. The brief overview is discussed here from relevant literature.

A Fast Algorithm for Multilevel Thresholding (Chen and Chung 2001)

Thresholding of an image is carried out to extract a target background from an image. Thresholding techniques are routinely based on grey level statistics of image on one dimensional(1D) histogram. Parametric and nonparametric methods (Abutaleb 1989; Tsai and Chen 1992; Yen et al. 1995) are used for finding thresholds. Image pixels are classified into separate bright and dark groups. Maximum peaks of these two bright and dark group pixels are used for finding threshold in parametric methods. In nonparametric methods for example, Otsu's method (Otsu 1979) chooses the optimal thresholds by maximizing between-class variance with an exhaustive search.

An image consists of 2D gray scale intensity function with N pixels with gray levels from 1 to L. The probability for gray level, i is denoted by

$$p_i = \frac{f_i}{N} \tag{1}$$

Where, p_i is probability for gray level i f_i is number of pixels with gray level i

To segment an image into M classes, Otsu's method predicts M-1 thresholds$\{t_1,t_2,t_3,\ldots t_{M\text{-}1}\}$. The gray levels for each of M classes are $[1,\ldots,t_1]$ for class C_1 $[t_1+1,\ldots,t_2]$ for class C_2 $[t_{i\text{-}1} + 1, \ldots ., t_i]$ for class C_i …. and $[t_{M\text{-}1}+1, \ldots., t_M]$ for class C_M

The optimal thresholds $\{t_1, t_2, t_3\ldots. t_{M\text{-}1}\}$ are chosen by maximizing between-class variance σ_B^2 as follows:

$$\sigma_B^2(t_1, t_2, \ldots, t_{M-1}) = \sum_{k=1}^{M} \omega_k \mu_k^2 - \mu_T^2 \tag{2}$$

Where, ω_k is zeroth-order cumulative moment of the kth class C_k

μ_k is first-order cumulative moment of the kth class C_k defined as follows:

$$\mu_k = \sum_{i \in C_k} i p_i$$

Downloaded from http://onepetro.org/SPEADIP/proceedings-pdf/22ADIP/1-22ADIP/D012S145R004/3045811/spe-211691-ms.pdf by China University of Petroleum (East China) user on 08 July 2023

μ_T is mean intensity for the whole image defined as follow:

$$\mu_T = \sum_{k=1}^{M} \omega_k \mu_k$$

Since the second term in equation 2 is independent of the choice of the thresholds, optimal thresholds $\{t_1^*, t_2^*, \ldots \ldots .t_{M-1}^*\}$ can be chosen by maximizing a modified between-class variance $\sigma_B'^2$ defined as follow:

$$\sigma_B'^2 = \sum_{k=1}^{M} \omega_k \mu_k^2 \tag{3}$$

The optimal threshold values $\{t_1^*, t_2^*, \ldots \ldots .t_{M-1}^*\}$ are predicted by maximizing a modified between-class variance $\sigma_B'^2$

$$\{t_1^*, t_2^*, \ldots \ldots .t_{M-1}^*\} = \mathbf{Arg}\ \ \mathbf{Max}\{\sigma_B'^2(\{t_1^*, t_2^*, \ldots \ldots .t_{M-1}^*\})\} \tag{4}$$

Fast algorithm for multilevel thresholding based on improved Otsu method is programmed in python for processing of photomicrographs of petrographic thin sections for digital reservoir description.

Augmented K-means clustering for Multilevel Image Segmentation

Original Otsu method and improved Otsu methods as above are widely used for image segmentation as these algorithms are simple and faster. However, extending these algorithms to multilevel image segmentation is complicated as the choice of thresholds demands multiple iterations for computing zeroth and first order moments. It is further complicated when these are applied to geological images such as photomicrographs of thin sections. The color and pixel intensities are very heterogenous due to chemical compositions of minerals and tone changes due to stress induced deformation and diagenetic alternations. Therefore, thresholding methods need to be augmented to yield satisfactory results particularly for heterogenous thin section images from carbonates reservoirs.

Clustering techniques are the potential alternatives to thresholding methods due to their multi-dimensional nature as an extension for multilevel image segmentation. Clustering is an unsupervised learning method to define finite set of clusters to classify pixels in an image. K-Means algorithm is one of the popular clustering methods due to its simplicity and low computational cost. Prior knowledge of number of clusters is required to classify pixel intensities based on intra-cluster similarity maximization and inter-cluster similarity minimization. Euclidean distance is computed to assign pixels to respective clusters in K-Means clustering method. The critical elements of K-Means algorithm are prior definition of number of cluster and initialization procedure. Improper initialization results in dead centers with no pixels. In such situations, it is challenging to differentiate dead centers and clusters with zero intra-cluster variance.

There are improved algorithms in the literature to overcome the shortcomings with conventional K-Means clustering. Pixel Intensity Clustering Algorithm (PICA) (Olugbara et al. 2015) is one of those improved methods addressing the issues with initialization of K-Means clustering. PICA broadly involves three steps. First step is initialization of cluster centroids based on linear partitioning of image pixel intensities. Linear partitioning helps to avoid dead centers by a guesstimate of initial cluster centroids through appropriate cluster weights. In the second step, the remaining pixel intensities which are not associated to any initial cluster centroid are now allocated to suitable clusters based on maximization of between-cluster variance. In the third step, segmented image is generated by utilizing input image as reference through reconfiguration process. The reconfiguration process involves assigning the pixel intensity at each spatial location in output image with centroid of cluster to which the pixel intensity in the input image belongs. PICA method addressed the shortcomings with conventional K-Means clustering. But PICA method warrants a two-dimensional gray scale image as input with desired clusters. This assumption disallows PICA method for

Downloaded from http://onepetro.org/SPEADIP/proceedings-pdf/22ADIP/1-22ADIP/D012S145R004/3045811/spe-211691-ms.pdf by China University of Petroleum (East China) user on 08 July 2023

direct application on geological image samples such as thin sections. Thin sections are colored images with heterogonous pixel intensities. The pore space in thin section is impregnated with blue-dyed epoxy resin and matrix is stained with alizarin Red S and potassium ferricyanide for carbonate mineral identification.

Hence in proposed workflow, conventional K-Means algorithm is re-programmed in python for multilevel image segmentation by addressing the key issues of initial number of clusters and initialization procedure. Alternative ways to address the key issues have been incorporated while re-programming conventional K-Means clustering. Firstly, the number of clusters is defined based on elbow method. In the elbow method, the variance which is Within-Cluster Sum of Squared errors (WCSS) is plotted against the number of clusters. The optimal number of clusters is found out from the elbow point on the plot of WCSS and number of clusters. With that, number of clusters can be determined with reasonable accuracy. Initialization procedure is a critical step in K-Means clustering to avoid incidence of dead centers. Instead of arbitrary selection of initial cluster centroids, initialization is carried out with careful seeding weighted by specific probability as proposed in K-Means++ algorithm (Arthur and Vassilvitskii 2007).

For given input image with n pixel intensities in χ, k number of initial cluster centroids $C = \{c_1, c_2, \ldots, c_k\}$ can be chosen by minimizing the potential function (Φ) defined as below.

$$\Phi = \sum_{x \in X}^{n} \min_{c \in x} ||x - c||^2 \tag{5}$$

K-Means++ clustering works as follows by augmenting conventional K-Means through careful seeding for initialization. Let ***D(x)*** denote the shortest distance from data point × to the closest center.

1. Choose an initial center $\boldsymbol{c}_1$ uniformly from χ
2. Choose the next center $\boldsymbol{c}_i$ for $c_i = x \in \chi$ with probability $\dfrac{D(x)^2}{\sum_{x \in \chi}^{n} D(x)^2}$ called as D^2 weighting
3. Repeat step 2 until k number of initial cluster centroids
4. For each i ∈{1,…,k}, set the cluster $\boldsymbol{c}_i$ to be the set points in χ that are closer to $\boldsymbol{c}_j$ for all $\boldsymbol{j \neq i}$
5. For each i ∈{1,…,k}, set $\boldsymbol{c}_i$ to be the center of mass for all points in $\boldsymbol{C}_i$: $c_i = \dfrac{1}{|c_i|} \sum_{x \in C_i}^{k} x$
6. Repeat step 4 and 5 until C no longer changes

Workflow and Application

Multilevel thresholding and augmented K-Means clustering are considered for developing this workflow in python. Multilevel thresholding method is followed for image processing of thin section images which are less heterogenous. Quantitative reservoir description is carried out on segmented image by multilevel thresholding. Augmented K-means clustering is performed on heterogenous thin section images. In next step, clusters belong to background matrix were filtered for the sake of reprocessing filtered grayscale image through multilevel thresholding for quantitative reservoir description. Figure 2 shows automated image processing workflow with detailed steps as a flow chart

Downloaded from http://onepetro.org/SPEADIP/proceedings-pdf/22ADIP/1-22ADIP/D012S145R004/3045811/spe-211691-ms.pdf by China University of Petroleum (East China) user on 08 July 2023

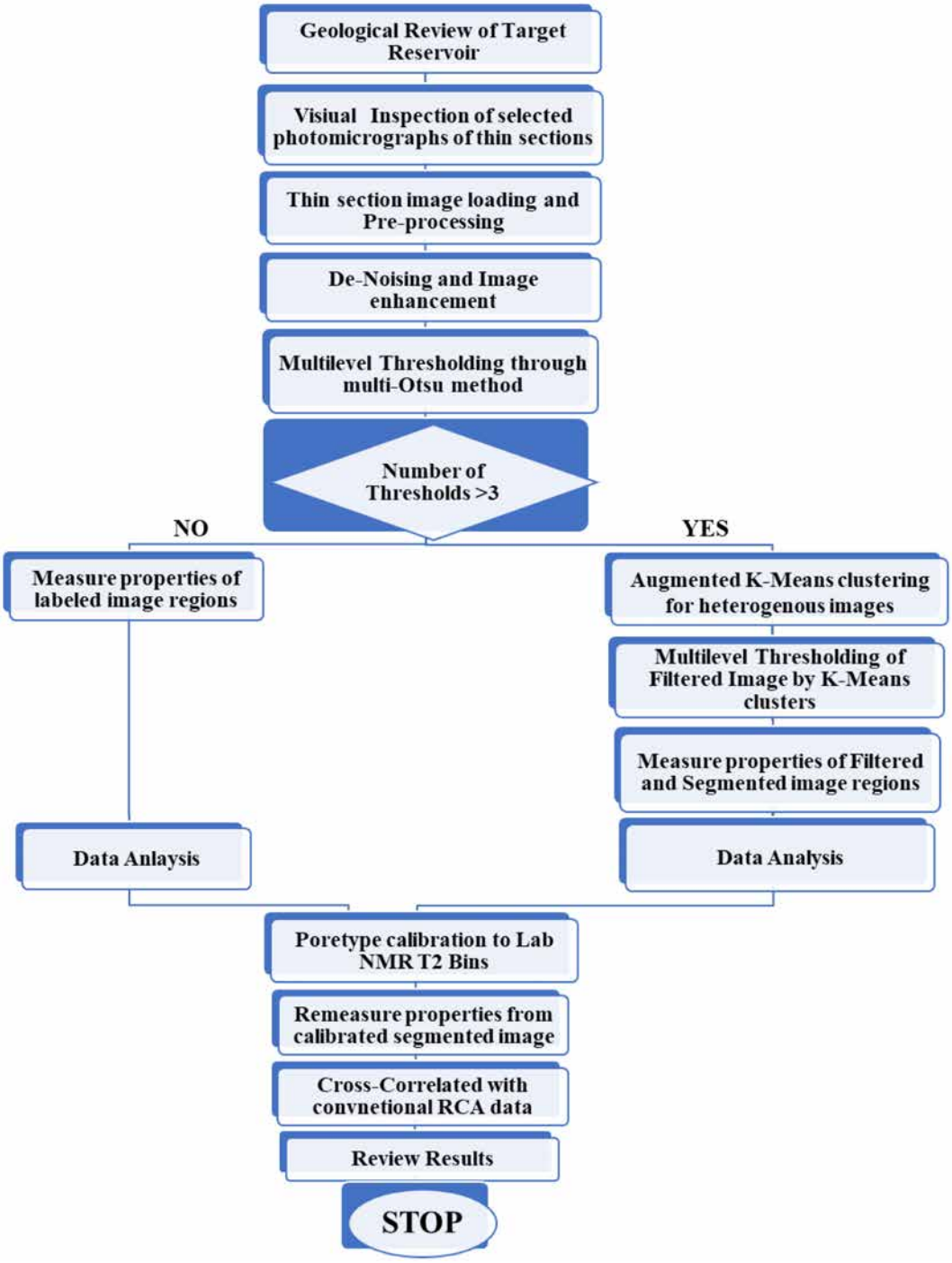

Figure 2—Flow chart for automated image processing workflow

Application of automated image processing workflow is demonstrated with a casestudy from heterogenous carbonate reservoir belong to onshore field, Abu Dhabi. Target reservoir is dominantly a limestone with traces of dolomite. A typical log composite is shown in Figure 3 across target reservoir in well X. Target reservoir is subdivided into two subzones with lower porous zone(Z1) at the top separated by dense stylolite from higher porous zone(Z2) below. The average porosity is 8% in Z1 and 21% in Z2. Core calibrated permeability log in Track 8 of Figure 3 indicate higher permeability at the top of Z2 and lower permeability at the bottom of Z2. Thin section samples are acquired in Z2 at the locations (Solid dots) shown in Track 6 of Figure 3 from conventional core of well X. Thin section samples are chosen such the red solid dots belong to higher permeability intervals at the top of Z2 and non-red solid

Downloaded from http://onepetro.org/SPEADIP/proceedings-pdf/22ADIP/1-22ADIP/D012S145R004/3045811/spe-211691-ms.pdf by China University of Petroleum (East China) user on 08 July 2023

dots belong to lower permeability intervals from bottom of Z2. Geological review of target reservoir is carried out to understand expected depositional and diagenetic constituents in thin section images before proceeding to image processing. Paragenetic sequences are studied from conventional sedimentological descriptions to understand their impact on texture, diagenetic fabric, and pore type. Pore space in the samples is impregnated with blue-dyed epoxy resin and stained with Alizarin Red S and Potassium Ferricyanide for carbonate mineral identification. These staining techniques on thin sections develop distinguishable colors on photomicrographs. In general, pink color denotes non-ferroan calcite, purple color denotes the presence of ferroan calcite and unstained crystals are non-ferroan dolomite. High quality photomicrographs under plane polarized light are generated using 45x magnification for acquired 23 thin section samples form target reservoir in well X. All the 23 thin section samples have a parent core plug having routine core analysis (RCA) data i.e., porosity and permeability measurements. All parent core plugs also have special core analysis (SCAL) data mainly laboratory NMR T2 distributions and mercury injection capillary pressure (MICP)

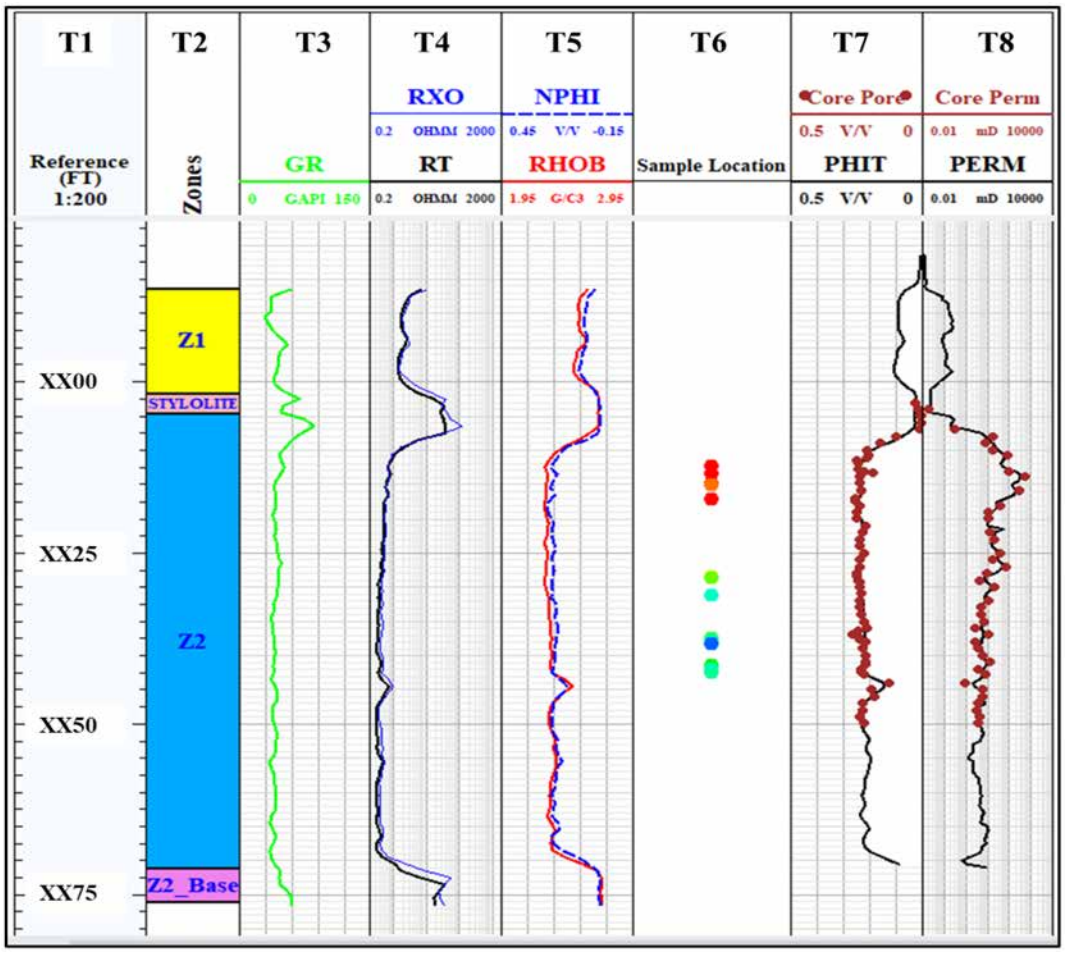

Figure 3—Typical Log composite for target reservoir in well X showing thin section locations (T1: Depth; T2: Zones; T3: Gamma (GR); T4: Deep resistivity (RT)/Shallow resistivity (RXO); T4: Bulk density (RHOB)/Neutron (NPHI); T5: Sample location; T6: Log porosity (PHIT)/Core porosity (Core Pore); T7: Log permeability (PERM)/Core permeability (Core Perm))

Initial geological review of target reservoir suggested dominantly grain supported carbonates (grainstones and packstones) and mud supported wackstones in some intervals. Key granular components include peloids as dominant one followed by intraclasts and benthonic foraminifers. Important diagenetic controls are dissolution and cementation introducing heterogeneity in target reservoir. A visual inspection on few selected samples validated the comments from initial geological review.

Downloaded from http://onepetro.org/SPEADIP/proceedings-pdf/22ADIP/1-22ADIP/D012S145R004/3045811/spe-211691-ms.pdf by China University of Petroleum (East China) user on 08 July 2023

Thin section photomicrographs were evaluated for dimensions and scale before importing to the workflow. De-noising is carried out on all images to preserve texture. Non-local means denoising is performed for this workflow. Non-local means algorithm (Buades et al. 2005) is well suited for thin section images which usually have specific textures.

Morphological operators are carried out on all thin section images for image enhancement. Morphological operations are mainly erosion and dilation techniques for removing noise, seclusion of isolated elements, joining of disparate elements and to find intensity bumps by treating missing pixels.

The next step is image segmentation and labeling. The objective of image segmentation is to separate background matrix, granular elements, cements, and pores. In this paper, the emphasis is on pore space, granular elements, and cement to extract controlling parameters on reservoir heterogeneity for digital reservoir description. Multilevel thresholding using Multi-Otsu method is performed to segment images and labeled them as per thresholds. If the predicted thresholds are more than 3 and if the thin section image is heterogenous, the decision is made to re-run image processing using augmented K-Means clustering.

For the heterogenous thin section images, image segmentation is conducted in two steps, first by augmented K-Means clustering for predicting clusters of similar pixel intensities. Later, the clusters corresponding to background matrix are filtered out leaving the clusters of pixels corresponding to pore space and cement/granular elements. The filtered image is now a 2D gray scale image after removing background matrix. The filtered image in second step is segmented by multilevel thresholding. This two-step process overcome the limitations in extending multilevel thresholding techniques to heterogenous thin section images. Image labeling is an important step to label the segmented regions as per thresholds predicted by comparing with original thin section image. The labeled elements are denoted as per geological elements such as matrix, pores, cement, and granular content. The next stage in image processing is to measure geometrical properties of labeled regions in thin section photomicrographs using mathematical algorithms (Burger 2009). The measured geometrical and physical properties are area, equivalent diameter, perimeter, solidity, eccentricity, and entropy. Reservoir properties are derived from the measured geometrical properties of labeled images. The derived reservoir properties are 2D-Porosity, polymodal pore size distribution, mean pore size, cement, and granular contents for each thin section image. Data analysis is carried out on the measured and derived datasets for consistency and anomalies.

A direct correlation between 2D reservoir properties from thin sections and 3D reservoirs properties from routine core analysis is not recommended in heterogenous carbonate reservoirs. Therefore, a novel method is presented here as additional step in the proposed image processing workflow for the integration between 2D reservoir properties from thin sections and 3D reservoirs properties from core plugs. Laboratory NMR data is utilized in this step for the bridge between image processing results and conventional core analysis data. Laboratory NMR provide distributions of transverse relaxation time (T2) of protons under oscillating magnetics field on core plugs saturated with reservoir brine. T2 distributions for brine saturated plug imitates inherent pore size distributions whereas mercury injection capillary pressure (MICP) data indicate pore throat distributions. The derived polymodal pore size distributions from image processing are compared with laboratory NMR T2 distributions and MICP data. It is observed that inferred pore types from polymodal pore size distributions are correlating well with laboratory NMR T2 distributions by a constant of proportionality on pore size axis. This constant of proportionality equivalent to surface relaxivity(ρ) of pore surface is applied to calibrate each thin section image. The calibrated image now has polymodal pore size distributions calibrated to laboratory NMR T2 distributions at plug scale.

Image segmentation followed by measurement of 2D geometrical properties is repeated for all thin section images such that estimated 2D reservoir properties honor inherent pore types and reservoir heterogeneity observed in core plugs. Calibrated 2D reservoir properties are correlated with equivalent reservoir properties from routine core analysis data. A comprehensive candidate rock typing (CRT) is carried out exclusively based on digital descriptive data. Automated image processing results are reviewed as per CRT to develop digital proxy reservoir quality parameters to understand reservoir heterogeneity in target reservoir(Z). The

Downloaded from http://onepetro.org/SPEADIP/proceedings-pdf/22ADIP/1-22ADIP/D012S145R004/3045811/spe-211691-ms.pdf by China University of Petroleum (East China) user on 08 July 2023

limitation of this novel workflow is also investigated and explained in discussion section. The workflow and application are further elaborated in results section with illustrative figures for each step using thin section images of target reservoir(Z).

Results

Automated image processing workflow is programmed in python and evaluated 23 photomicrographs in a loop for digital reservoir description of target reservoir(Z). All 23 photomicrographs have 4.2 um/pixel scale. The workflow pre-requisite high quality image for thin section samples. Initial geological review of target reservoir indicated grain supported carbonates with visible intergranular porosity as shown in Figure 4 & Figure 5.

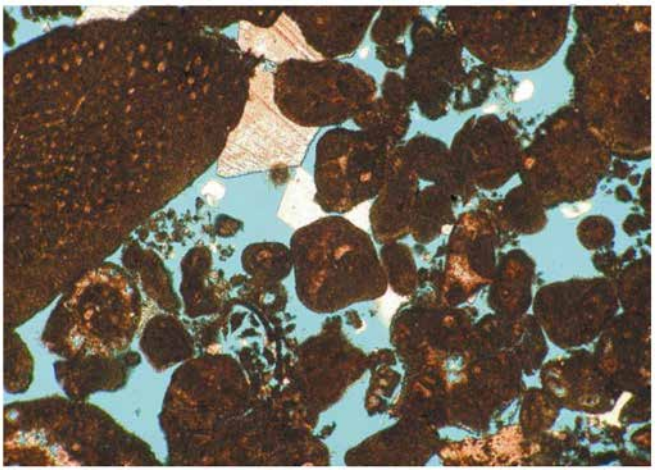

Figure 4—Sample microphotograph(A) for grainstone in target reservoir

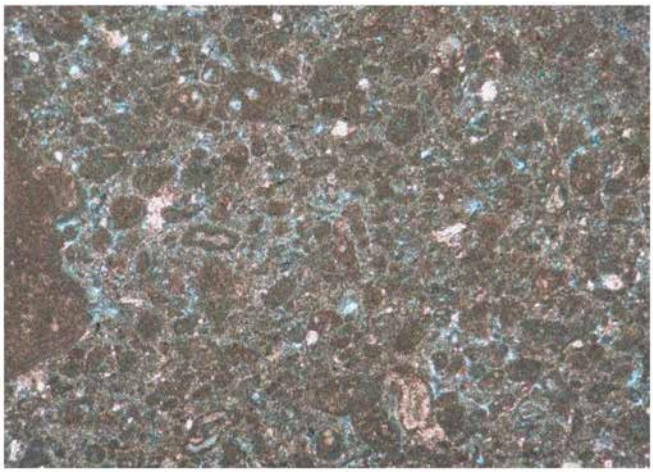

Figure 5—Sample microphotograph(B) for grain supported packstone in target reservoir

Figure 4 shows poorly cemented intraclastic grainstone with good visible porosity displayed in blue due to resin impregnation on thin section sample(A). The pink stained are calcite and unstained(white) are dolomite. Figure 5 shows a peloidal packstone/grainstone with moderate visible porosity in thin section sample(B). Intergranular pores are enlarged by dissolution processes. Micritic grains have microporosity as indicated by the blue color due to resin impregnation.

Preprocessing of the thin section images resulted in enhanced image pixel resolution by applying denoising algorithms and morphological operators.

Downloaded from http://onepetro.org/SPEADIP/proceedings-pdf/22ADIP/1-22ADIP/D012S145R004/3045811/spe-211691-ms.pdf by China University of Petroleum (East China) user on 08 July 2023

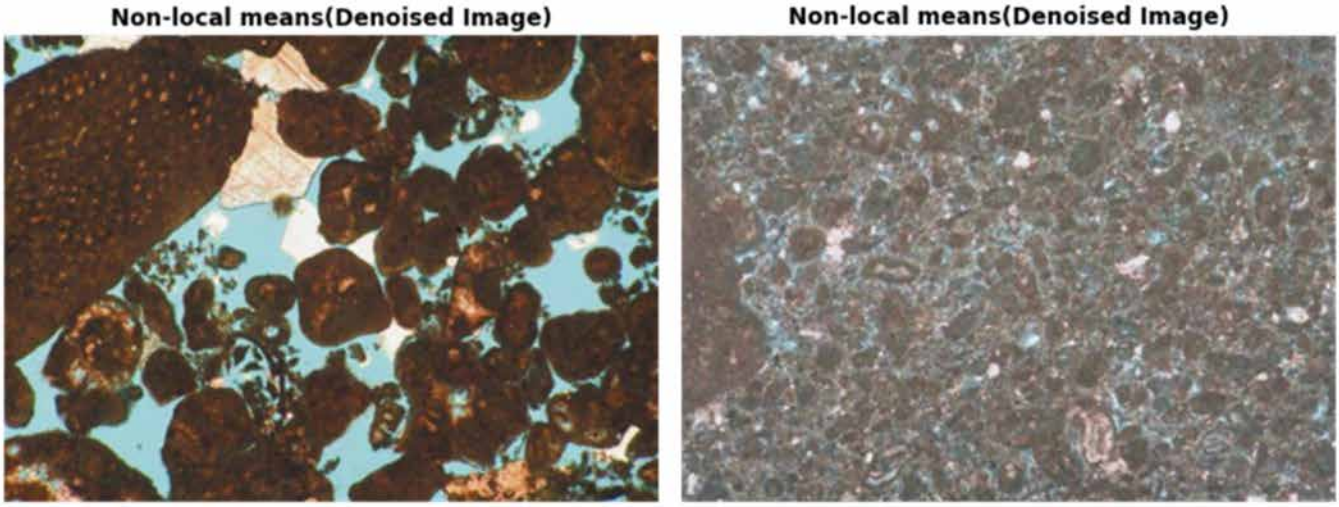

Figure 6 shows an example for the results of denoising by non-local mean algorithm. The difference between original image and denoised image is not visual by naked eye. But at pixel intensity level, an improvement in peak signal noise ratio (PSNR) by 10- 40% is achieved compared to original image by treating missing pixels, boundaries and avoiding intensity bumps.

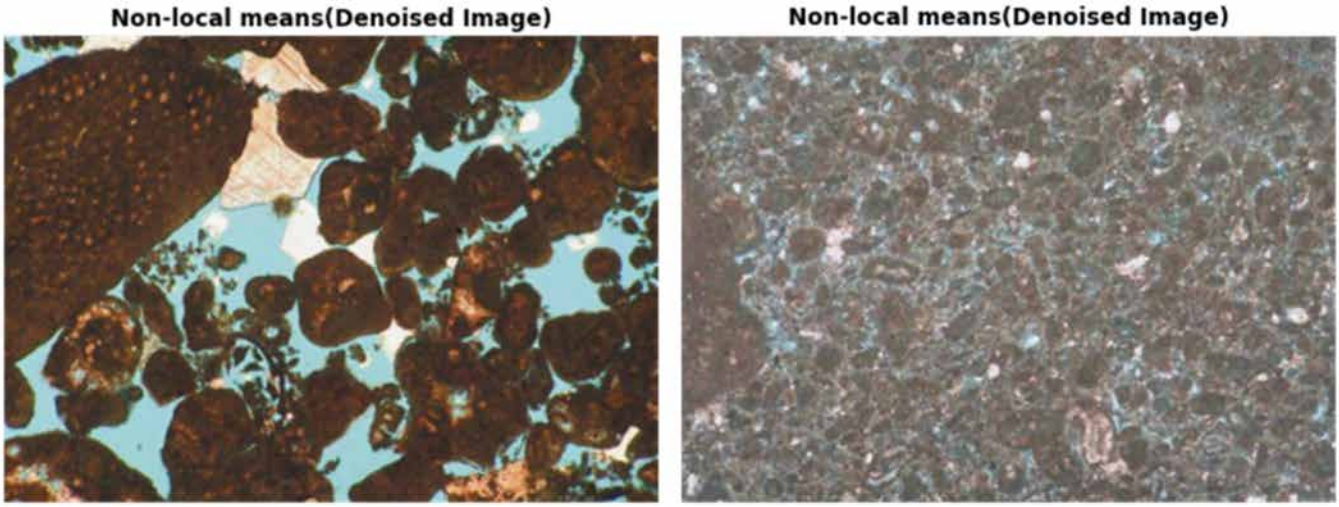

Figure 6—Image enhancement after denoising for a thin section image (A & B)

Results of image segmentation by multilevel thresholding is displayed in Figure 7 for thin section sample(C). The initial results are shown in Figure 7 for segmented image(C) with background matrix in dark color with abundant peloids and intraclasts. Remaining pores and cement are interpreted in green to yellow color. The segmented sample(C) is color-coded as per individual segments and are labeled as per geological elements in Figure 8. The pore space is scaled as per abundance of connected pixel area in right of Figure 8. From labelled image in right of Figure 8, it is interpreted that carbonate dissolution is the key diagenetic process which developed oversized pores. The gray color in labeled image specify calcite cementation present as rim around grains and as overgrowth. Highlights from Figure 7 & Figure 8 Figure 8 are that thin section sample(C) is expected to have good reservoir properties due to interconnected pores and lower cementation in intergranular area.

Downloaded from http://onepetro.org/SPEADIP/proceedings-pdf/22ADIP/1-22ADIP/D012S145R004/3045811/spe-211691-ms.pdf by China University of Petroleum (East China) user on 08 July 2023

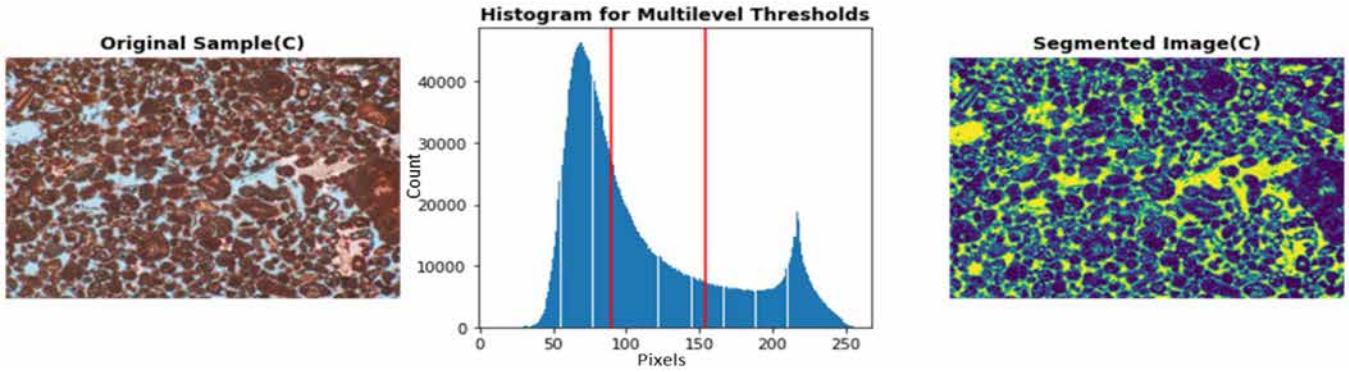

Figure 7—Multilevel image thresholding and segmentation of image sample(C)

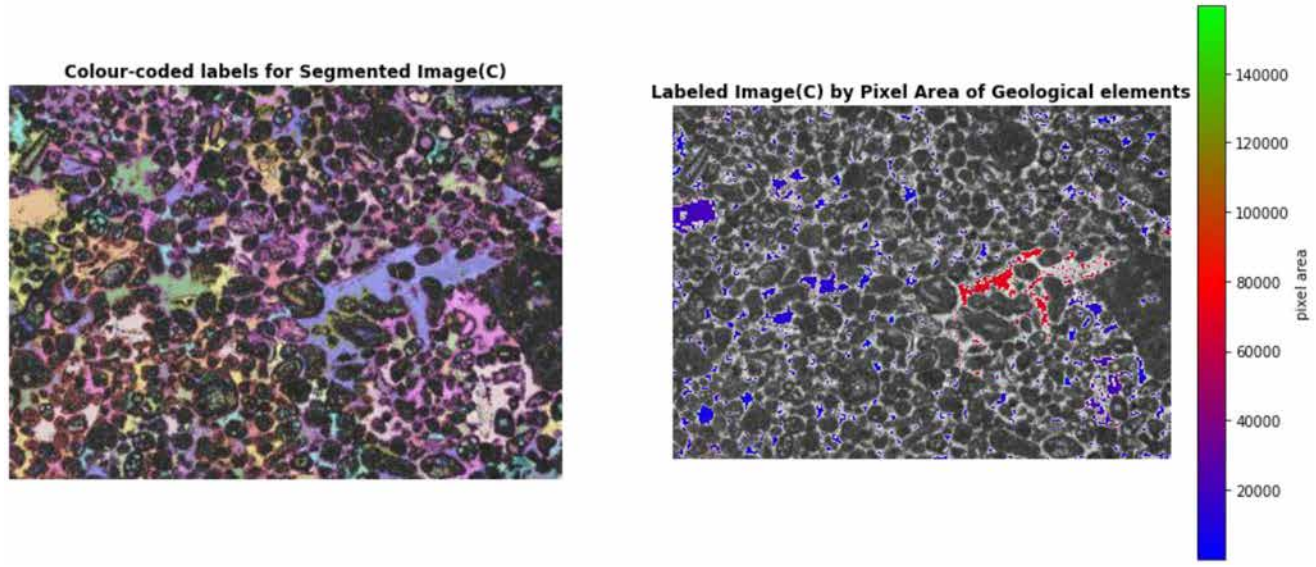

Figure 8—Labeled Image Sample(C)

As heterogenous samples requires thresholds greater than three, augmented K-Means clustering is performed for optimal clustering in heterogenous images. Later image segmentation is conducted on filtered image after removing background clusters. Thin section sample(D) in left of Figure 9 is one such thin section image with heterogenous pixel intensities due to abundant peloids and micritized grains. Elbow method is used to find optimal clusters in thin section sample(D) prior to image segmentation. Six dominant clusters are found in thin section sample(D) from right of Figure 9. The filtered image of thin section sample(D) (left of Figure 10) is further used for image segmentation by multilevel thresholds. The resulting segmented image captures pores and cements shown in green to yellow color in right of Figure 10.

Downloaded from http://onepetro.org/SPEADIP/proceedings-pdf/22ADIP/1-22ADIP/D012S145R004/3045811/spe-211691-ms.pdf by China University of Petroleum (East China) user on 08 July 2023

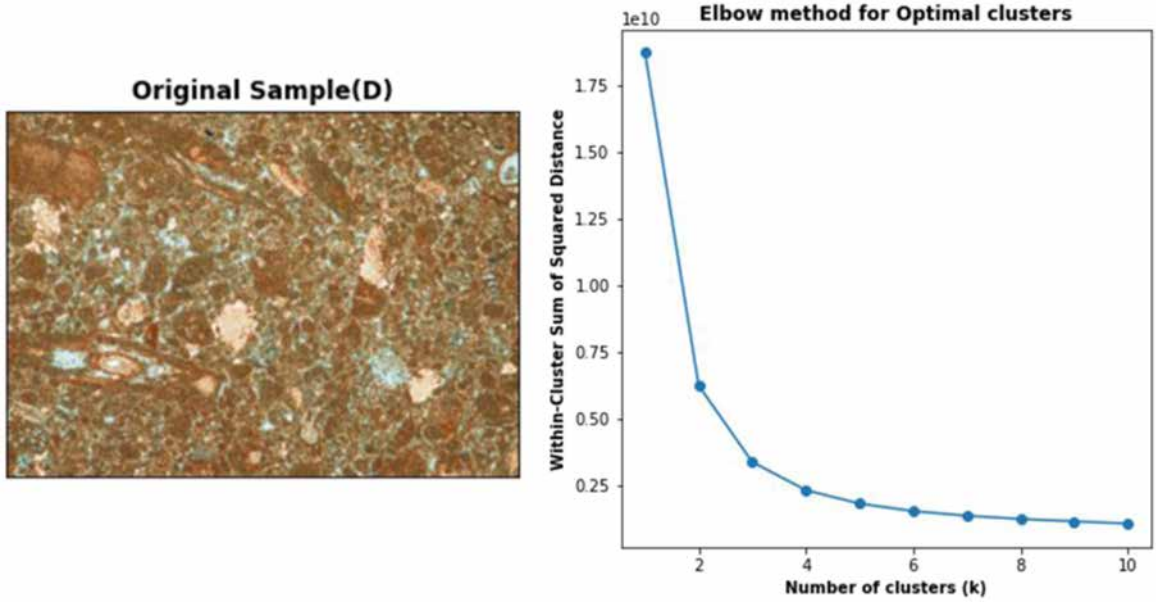

Figure 9—Augmented K-Means clustering on thin section sample(D)

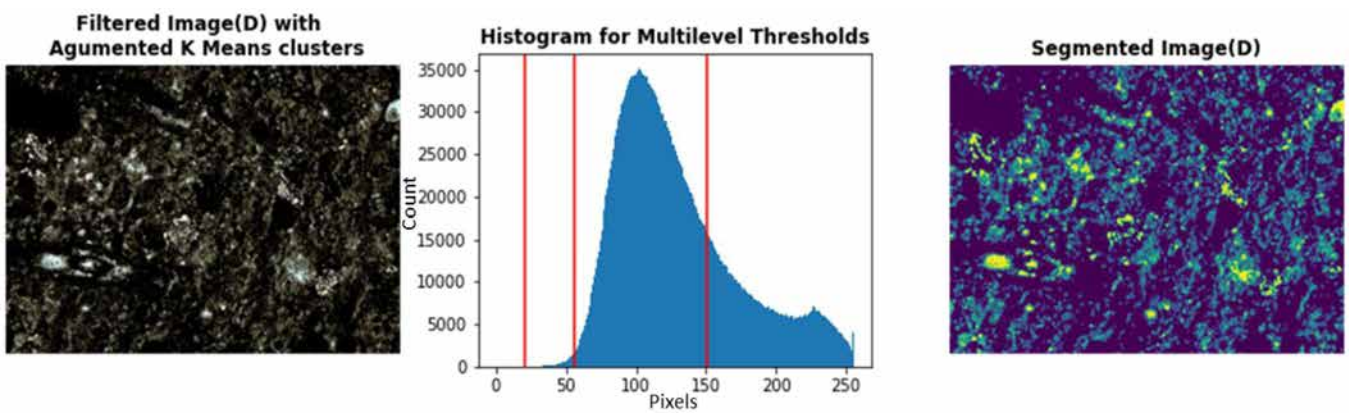

Figure 10—Multilevel image segmentation on filtered image of thin section samples(D)

The results so far are presented up to image segmentation step for both methods one example each for multilevel thresholding and augmented K-Means clustering respectively. The results for subsequent steps in the proposed workflow are common for both methods. Therefore, the results as demonstrated here after are for subsequent steps as examples from thin section sample(C) and thin section sample(D).

The segmented image required to be calibrated to known poretypes to measure 2D geometric properties for integration with 3D reservoir properties from conventional core plugs. Laboratory NMR on water saturated core plug is used as reference for generating a calibrated segmented image.

Poretypes derived from image processing and NMR T2 poretypes exhibits polymodal distributions in thin section sample(C). Figure 11 and Figure 12 illustrate cross-validation plots for both before and after calibration for thin section sample(C). Image derived poretypes and NMR T2 poretypes confirmed bimodal poretypes in thin section sample(C). The area weighted mean pore size is 1209 microns as shown by black dashed V-line in Figure 11 and Figure 12. The coefficient of surface relaxivity(ρ) is 1.65 um/ms from calibration coefficient. Similarly, Figure 13 and Figure 14 presents cross-validation plots for both before and after calibration for thin section sample(D). Image derived poretypes and NMR T2 poretypes confirmed uni-modal poretypes in thin section sample(D). The coefficient of surface relaxivity(ρ) is 0.65 um/ms for thin section sample(D). The area weighted mean pore size is 393 microns shown by black dashed V-line in

Downloaded from http://onepetro.org/SPEADIP/proceedings-pdf/22ADIP/1-22ADIP/D012S145R004/3045811/spe-211691-ms.pdf by China University of Petroleum (East China) user on 08 July 2023

Figure 13 and Figure 14. In the last step of proposed workflow, 2D geometrical properties are re-measured from calibrated segmented image using NMR T2 calibration.

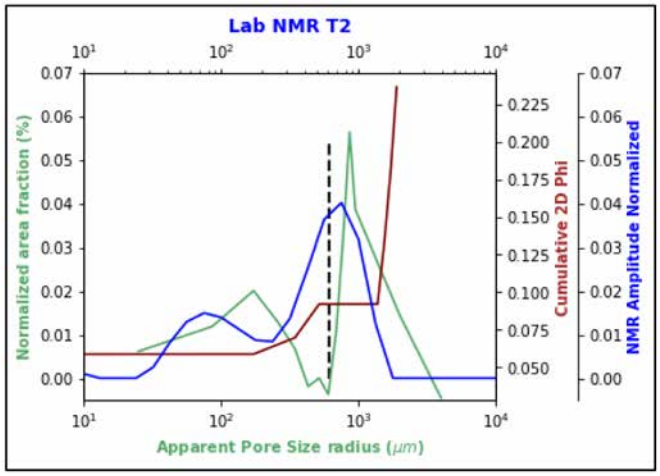

Figure 11—Cross-validation of 2D image poretypes with NMR poretypes before calibration for thin section samples(C)

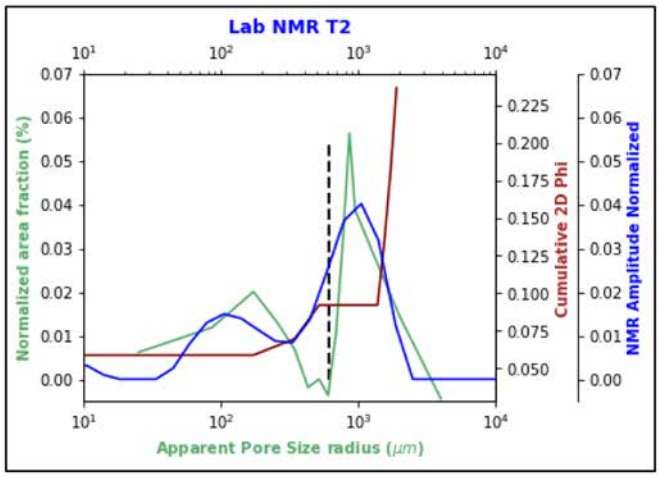

Figure 12—Cross-validation of 2D image poretypes with NMR poretypes after calibration for thin section samples(C)

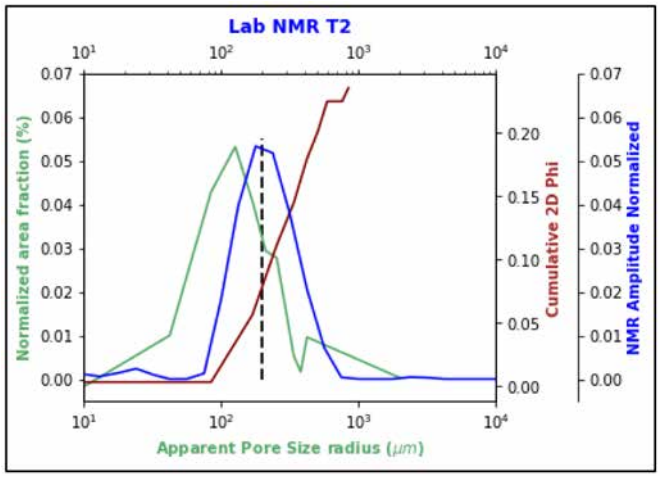

Figure 13—Cross-validation of 2D image poretypes with NMR poretypes before calibration for thin section samples(D)

Downloaded from http://onepetro.org/SPEADIP/proceedings-pdf/22ADIP/1-22ADIP/D012S145R004/3045811/spe-211691-ms.pdf by China University of Petroleum (East China) user on 08 July 2023

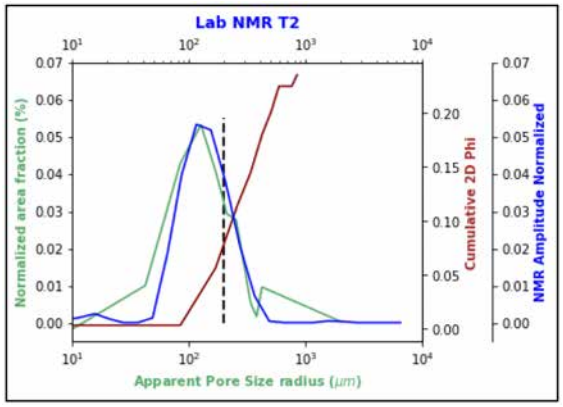

Figure 14—Cross-validation of 2D image poretypes with NMR poretypes after calibration for thin section samples(D)

The calibration process is conducted individually for all 23 thin section image samples of target reservoir with available Lab NMR T2 distributions. An example of digital descriptive dataset generated is shown in Table 1 for thin section samples A, B, C and D. Automated image processing is carried out on all the image samples by honoring complex carbonate poretypes and 2D reservoir properties are computed. Supplementary geometrical parameters namely, shannon entropy (Shannon, 1948), eccentricity and perimeter are derived from processed thin section images which are beneficial as digital proxy parameters in geoscience applications on rock typing. Shannon entropy is defined as measure of randomness in an image. In segmented image, shannon entropy indicates optical heterogeneity within pore space in thin section image. Similarly, eccentricity denotes whether segmented pores are circular or ellipsoidal. Perimeter is a measurement from integral geometry of all pores in segmented image.

Table 1—Digital descriptive data for thin sections A, B, C and D

Sample	PHI_2D (%)	Calcite Cement/Dolomite (%)	Matrix (%)	Weighted Mean Pore radius (microns)	Pore Size Array	Shannon Entropy	Eccentricity	Perimeter
A	20.9	2.9	76.2	468.6	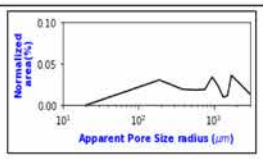	1.96	0.72	1012.2
B	25.5	9.1	65.4	66.1	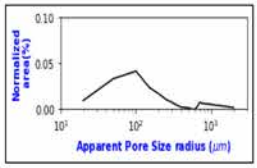	1.97	0.71	374.3
C	23.6	19.8	56.6	604.7	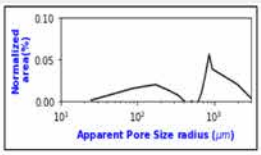	1.94	0.68	711.0
D	23.6	10.6	65.8	196.8	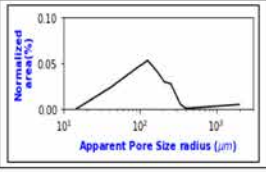	2.18	0.73	240.2

Downloaded from http://onepetro.org/SPEADIP/proceedings-pdf/22ADIP/1-22ADIP/D012S145R004/3045811/spe-211691-ms.pdf by China University of Petroleum (East China) user on 08 July 2023

The integration of 2D reservoir properties with 3D reservoir properties and potential application of digital thin section descriptive dataset in geological rock typing is discussed in next section.

Discussion

Automated image processing delivered a cross-validated digital thin section descriptive data. Polymodal pore size distributions are well correlated with poretypes from lab NMR T2. When attempted to calibrate with MICP pore throat distributions, it is found that polymodal pore size distributions are not comparable with MICP distributions. Figure 15 and Figure 16 present the comparison plots between thin section polymodal pore size and MICP pore throats for sample C and sample D respectively. Although MICP pore throats do exhibit bi-modal for sample C and uni-modal for sample D, MICP pore throat radius is not matched to thin section pore sizes. This is because pore throat radius is derived from mercury injection capillary pressure in MICP data whereas thin section pore sizes are physical measurements estimated from thin section image. Fundamentally, pore throats indicate capillarity in pores whereas pore sizes are geometrical parameters. Pore throat radius and pore size radius differ in perimeters for the same pores in geological samples. Therefore, MICP pore throats cannot be used as calibration for thin section descriptions as a bridge between 2D reservoirs properties and 3D reservoir properties of core plugs.

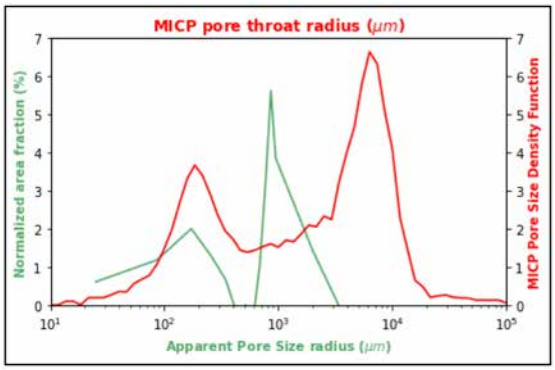

Figure 15—Comparison of MICP pore throat distribution with thin section derived pore size distributions for samples C

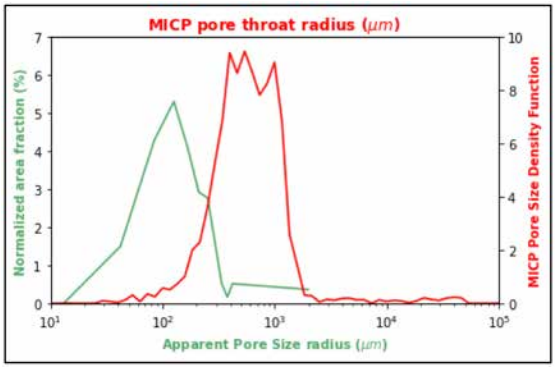

Figure 16—Comparison of MICP pore throat distribution with thin section derived pore size distributions for sample D

As all thin section samples are acquired from same core plug depths used in conventional core analysis, comparison is carried out between 2D reservoir properties and 3D reservoir properties. Figure 17 display the comparison of 2D porosity with core measured porosity. A good match is observed with respect to 1 on 1 line in Figure 17. Computation of 2D porosity from image processing is an efficient method instead of visual estimations in conventional workflows. Scale issues are observed for some thin section images causing differences between 2D porosity and core plug porosity. This is because of microscale heterogeneity

Downloaded from http://onepetro.org/SPEADIP/proceedings-pdf/22ADIP/1-22ADIP/D012S145R004/3045811/spe-211691-ms.pdf by China University of Petroleum (East China) user on 08 July 2023

seen on 2D thin section image which is not comparable to 3D core plug from which the thin section image is sampled.

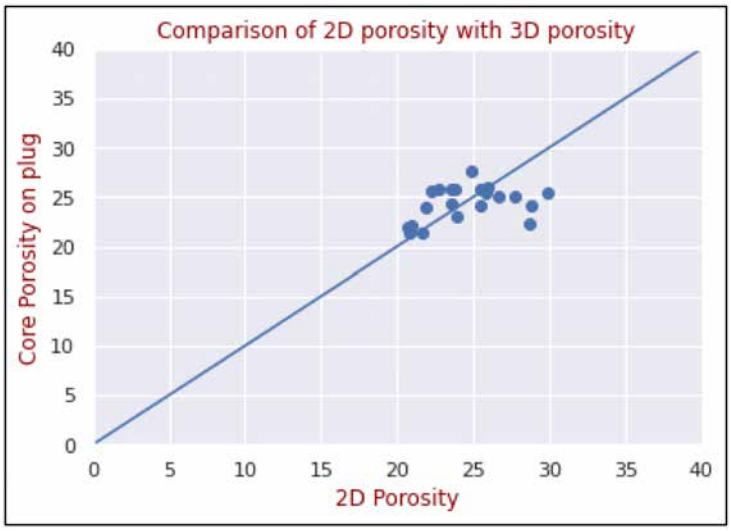

Figure 17—Comparison of 2D porosity with core porosity measured on core plugs

A preliminary rock typing is carried out independently with digital descriptive data of 23 thin section images of target reservoir. Two candidates rock types (CRT) were interpreted (Figure 18) using K-Means classification algorithm. Candidate rock types 1 exhibit bi-model poretypes as explained earlier with sample C whereas candidate rock types 2 exhibit uni-model poretypes as explained earlier with sample D in previous section. The workflow can be extended to a larger dataset of thin section images to develop a comprehensive candidate rock typing scheme by integrating with depositional history and lithofacies data. The merit of workflow is adding quantifiable and digital dimension in extracting descriptive data instead of text data from visual interpretation. The digital descriptive data can therefore be readily compatible to use in other standard geoscience workflows.

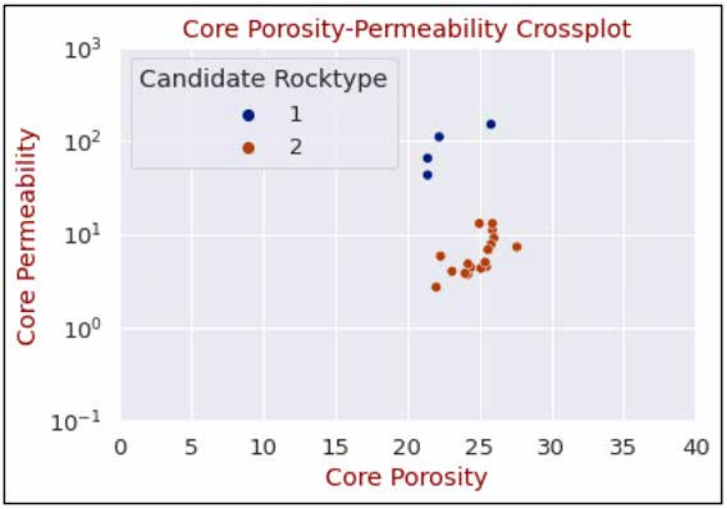

Figure 18—Candidate rock typing based on digital descriptive data from thin section images

Downloaded from http://onepetro.org/SPEADIP/proceedings-pdf/22ADIP/1-22ADIP/D012S145R004/3045811/spe-211691-ms.pdf by China University of Petroleum (East China) user on 08 July 2023

Digital descriptive data is amended with core analysis data from corresponding core plugs for each of thin section image in target reservoir. The core analysis data, mainly core permeability and lab T2 mean from core plugs amended to respective digital thin section data. Heatmap in Figure 19 highlights correlations among variables which are digital proxy reservoir quality parameters to understand reservoir heterogeneity. A cross-correlation of all variables in digital descriptive data according to candidate rock types revealed interrelationships and controlling parameters for reservoir heterogeneity in target reservoir. The cross-correlation is demonstrated by a pair plot in Figure 20. Core permeability has strong positive correlation with weighted mean pore size radius and perimeter of pores from thin section. Lab NMR T2 has moderate correlation with weighted mean pore size radius and perimeter of pores. Both core permeability and lab NMR T2 has low to moderate negative correlation with shannon entropy and eccentricity.

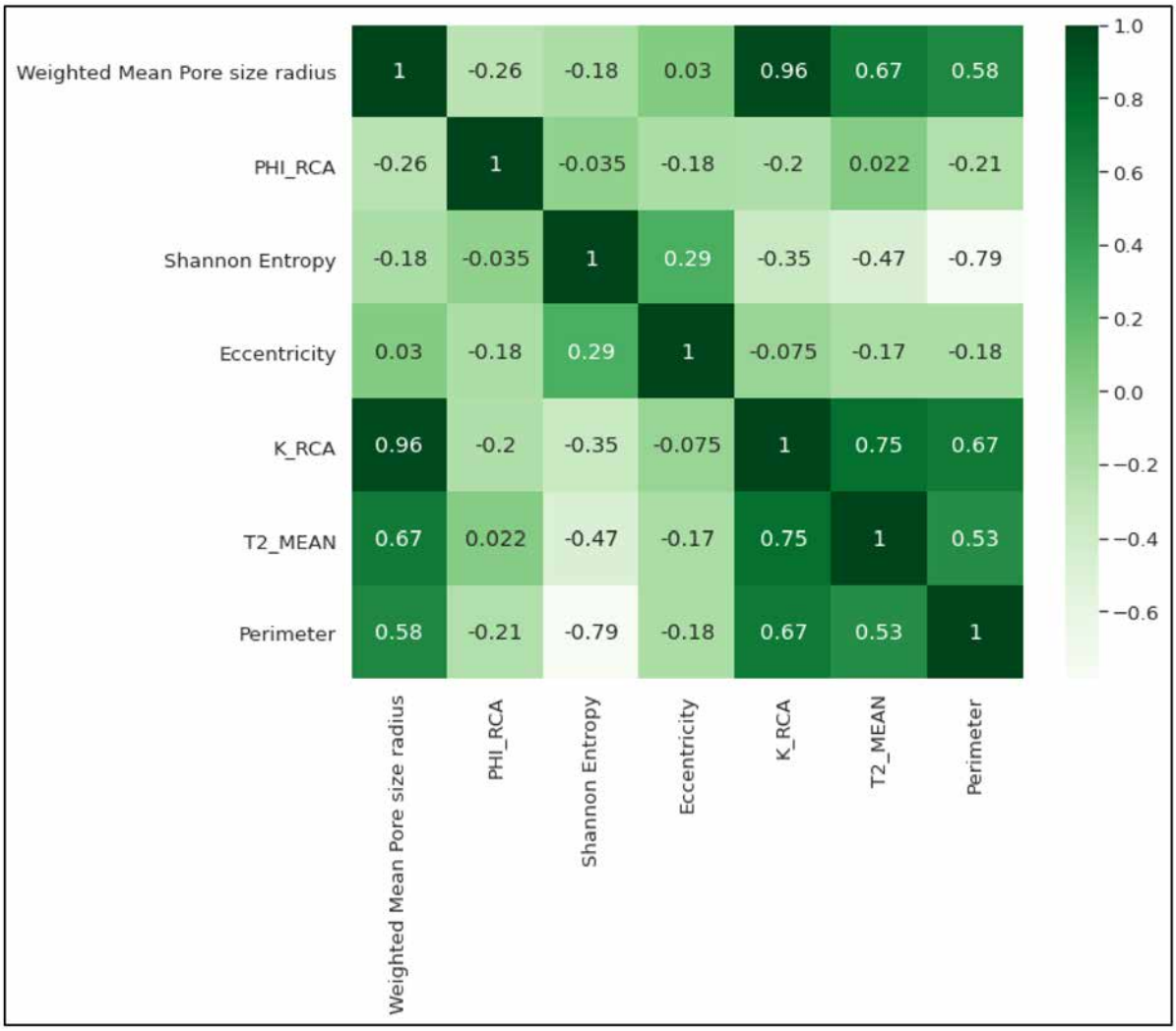

Figure 19—Heatmap of variables highlighting interrelationships as proxy parameters for rock typing

Downloaded from http://onepetro.org/SPEADIP/proceedings-pdf/22ADIP/1-22ADIP/D012S145R004/3045811/spe-211691-ms.pdf by China University of Petroleum (East China) user on 08 July 2023

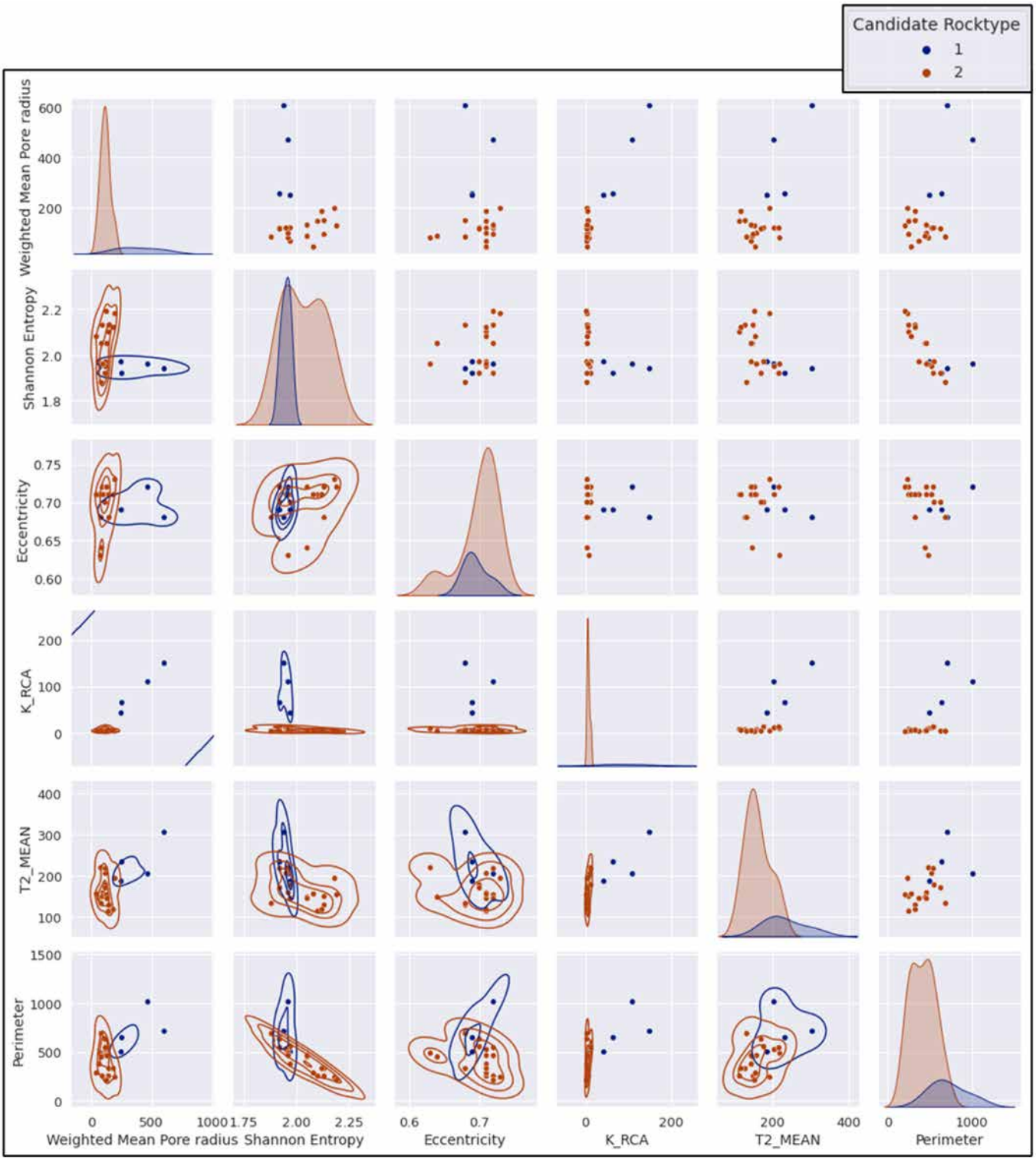

Figure 20—Cross-correlation of variables in amended thin section descriptive data

The limitation of demonstrated workflow is observed in instances when there is rapid change in reservoir heterogeneity at fine scale. Local carbonate diagenetic events make thin section image not comparable to its parent core plug. Figure 21 shows an example for rapid change in reservoir heterogeneity at fine scale. Three core plugs (S1, S2 & S3) and corresponding images were sampled at fine scale within 0.5 ft. CT scans of plugs indicate increased dense content as shown by increase in white color from S1 to S3. Corresponding thin section images too indicate increased dolomite shown by unstained crystals from S1 to

Downloaded from http://onepetro.org/SPEADIP/proceedings-pdf/22ADIP/1-22ADIP/D012S145R004/3045811/spe-211691-ms.pdf by China University of Petroleum (East China) user on 08 July 2023

S3. Efforts to bridge using available laboratory NMR for cross-validating 2D properties to 3D properties has no improvement on quantifiable accuracy of digital descriptive data. This is again due to NMR T2 at plug scale has no match with image derived polymodal pore size distributions (bottom of Figure 21). Figure 22 gives the results of automated image processing results without proper calibration for inherent pore types in respective plugs. Porosity profile from S1 to S3 is similar both in 3D measurements on core plugs and 2D measurements in thin section images. Likewise, permeability profile from S1 to S3 is well correlated with weighted mean of pore size radius from S1 to S3. The increase in grain density from S1 to S3 is cross validated with estimated dolomite content from 2D images. Figure 22 grossly illustrated a consistent data for the rapid change in heterogeneity at fine scale. But derived 2D reservoir properties and digital proxy reservoir quality parameters should be used carefully. This is reasoned due to mismatch between thin section image and its parent core plug.

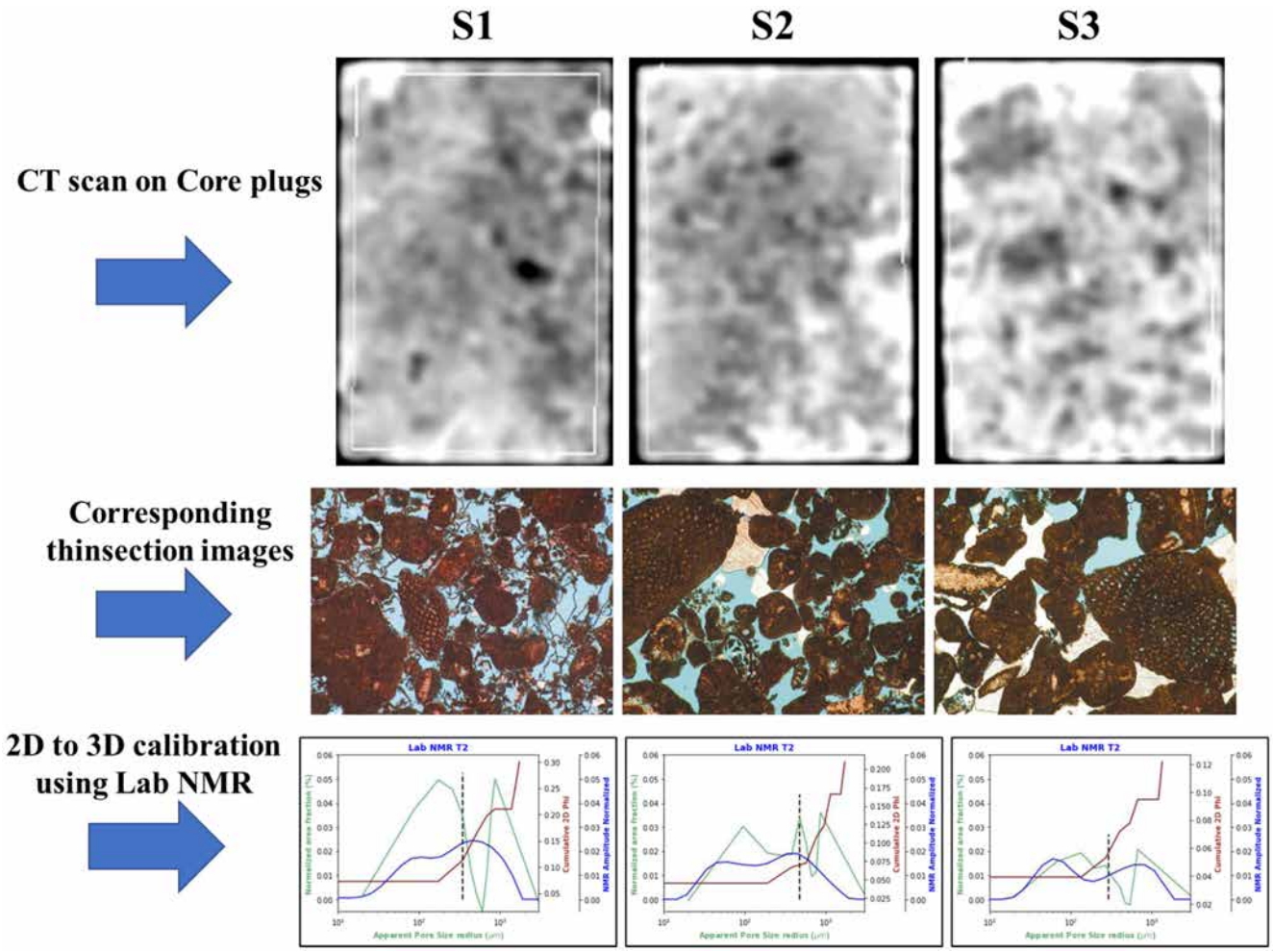

Figure 21—Example for limitation of workflow for rapid change in heterogeneity at fine scale

Downloaded from http://onepetro.org/SPEADIP/proceedings-pdf/22ADIP/1-22ADIP/D012S145R004/3045811/spe-211691-ms.pdf by China University of Petroleum (East China) user on 08 July 2023

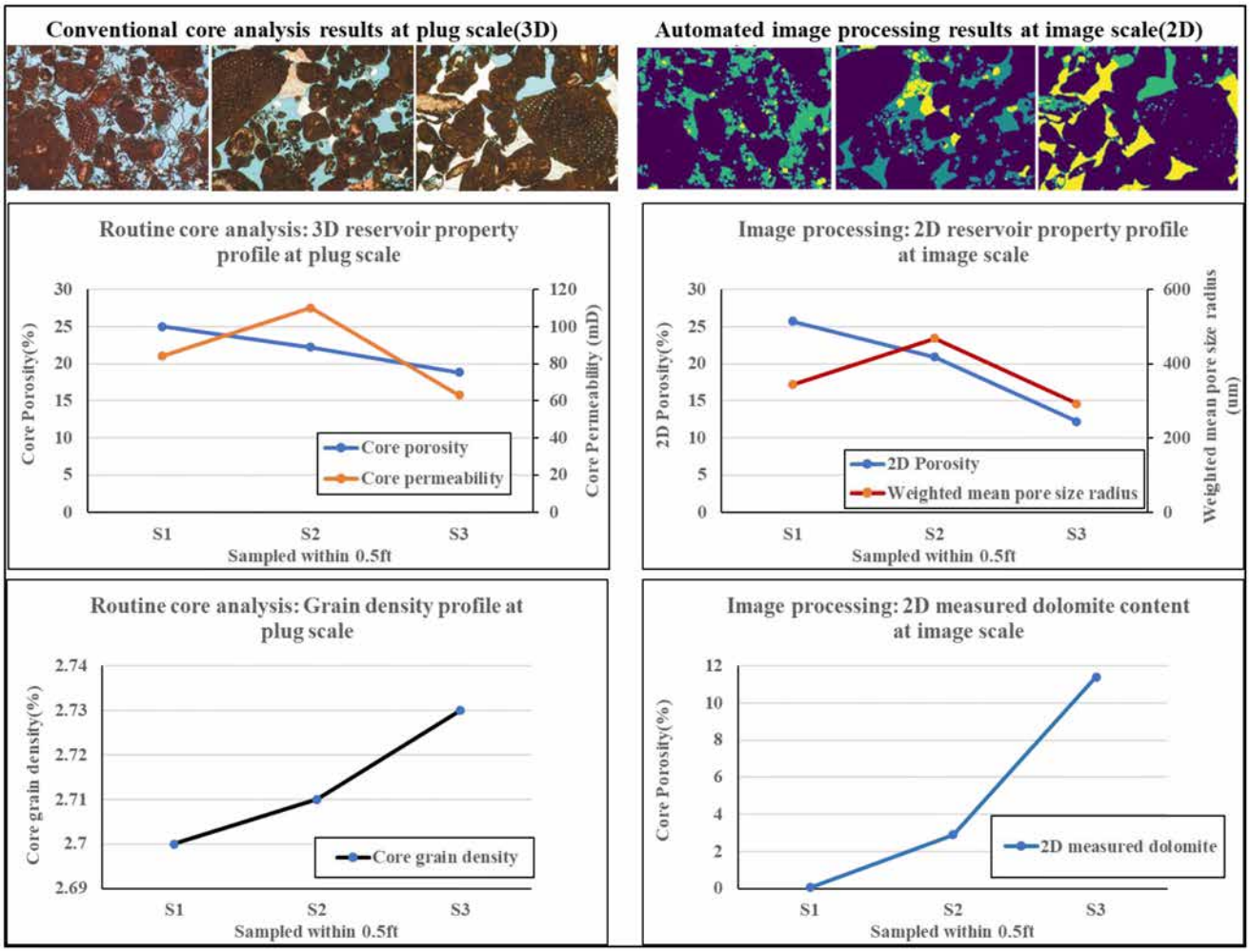

Figure 22—Comparison of routine core analysis results and image processing results for sampled plugs and corresponding images within 0.5ft

Conclusions

Automated image processing workflow is developed by leveraging image processing algorithms and computing power based on conventional reservoir characterization concepts. The novel workflow has an immense potential and scalable to large datasets by introducing an additional tool in contemporary reservoir characterization workflow. The key outcomes and recommendations are summarized as below.

- Automated image processing workflow produced a digital thin section descriptive data in place of visual interpretations in text format.
- The workflow is demonstrated with a casestudy extracting cross-validated digital reservoir properties from thin section depicting and honoring inherent reservoir heterogeneity
- The workflow offered a sophisticated and swift approach by uniting specialized fields of petrography, geology and petrophysics in extracting digital thin section descriptions compatible to conventional core analysis data.
- The calibration with NMR T2 made the bridge between 2D reservoir properties and 3D core plugs measurements which is lacking in previous image processing and conventional manual workflows.
- Future scope for automated image processing workflow is supposed to extend and develop a comprehensive candidate rock typing workflow integrating standard geoscience concepts.
- The scope of proposed workflow is not studied for mud-dominated rocks and shales

Downloaded from http://onepetro.org/SPEADIP/proceedings-pdf/22ADIP/1-22ADIP/D012S145R004/3045811/spe-211691-ms.pdf by China University of Petroleum (East China) user on 08 July 2023

Acknowledgments

The authors wish to thank and acknowledge the management of Abu Dhabi Company for Onshore Oil Operations (ADNOC Onshore) and Abu Dhabi National Oil Company (ADNOC), Abu Dhabi, for permission to publish this paper.

Nomenclature

NMR = Nuclear Magnetic Resonance
T2 = NMR transverse relaxation time[ms]
T1 = NMR longitudinal relaxation time[ms]
PSNR = Peak Signal Noise Ratio
MICP = Mercury injection capillary pressure
RCA = Routine Core Analysis
SCAL = Special Core Analysis
ρ = Coefficient of surface relaxivity

References

Abutaleb, A.S. 1989. Automatic thresholding of gray-level pictures using two-dimensional entropy, *Computer Vision, Graphics, and Image Processing*, Volume **47**, Issue 1, Pages 22–32, ISSN 0734–189X, DOI: https://doi.org/10.1016/0734-189X(89)90051-0

Bowers, M.C., Ehrlich, R., Howard, J.J. and Kenyon, WE. 1995. Determination of porosity types from NMR data and their relationship to porosity types derived from thin section *Journal of Petroleum Science and Engineering*, Volume **13**, Issue 1, Pages 1–14, ISSN 0920–4105, DOI: https://doi.org/10.1016/0920-4105(94)00056-A

Buades, A., Coll, B., Morel, J. 2005. A non-local algorithm for image denoising. *IEEE Computer Society Conference on Computer Vision and Pattern Recognition (CVPR'05)*, pp. 60–65 vol. **2**.

Burger, W., Burge, M. 2009. *Principles of Digital Image Processing: Core Algorithms*. Springer-Verlag, London.

Carr, M.B., Ehrlich, R., Bowers, M.C., Howard, J.J. 1995. Correlation of porosity types derived from NMR data and thin section image analysis in a carbonate reservoir. *Journal of Petroleum Science and Engineering*, Volume **14**, Issues 3–4, Pages 115–131, ISSN 0920-4105. DOI: https://doi.org/10.1016/0920-4105(95)00045-3

Chayes F., A. 1949. Simple point counter for thin section analysis, American Mineralogist. *Volume* **34**. Pages 1–11.

Delesse M. A. 1848. Procédé méchanique pour determiner la compositiondes roches, Annales des Mines. *Volume* **13**. Pages 379–388.

Ehrlich, R., and Horkowitz, J.P. 1987. Estimation of petrophysics from thin section: petrographic image analysis. *AAPG*, p. 238.

Ehrlich, R., Crabtree, J., Horkowitz, K. and Horkowitz, J. 1991a. Petrography and Reservoir Physics I: Objective Classification of Reservoir Porosity. *AAPG Bulletin* **75** (10). 1547–1562. DOI: https://doi.org/10.1306/0C9B2989-1710-11D7-8645000102C1865D

Gerard, R.E., Philipson, C.A., Manni, EM.et al. (eds.), *Automated Pattern Analysis in Petroleum Exploration* © Springer-Verlag New York Inc.

Gies, R.M., and McGovern, J.1993. Petrographic Image Analysis: An Effective Technology for Delineating Reservoir Quality." Paper presented at the SPE Gas Technology Symposium, Calgary, Alberta, Canada. DOI: https://doi.org/10.2118/26147-MS

Liao, P., Chen, T., & Chung, P.C. 2001. A Fast Algorithm for Multilevel Thresholding. *Journal of Information Science and Engineering*., **17**, 713–727.

Olugbara, O.O., Adetiba, E., Oyewole, A.S. 2015. Pixel Intensity Clustering Algorithm for Multilevel Image Segmentation. *Hindawi Publishing Corporation Mathematical Problems in Engineering*, Volume **2015**, Article ID 649802, 19 pages. DOI: http://dx.doi.org/10.1155/2015/649802

Otsu, N. 1979. A threshold selection method from gray level histograms. *IEEE Transactions on Systems, Man, and Cybernetics*, **9**, 62–66.

Shannon, C. E. 1948. A mathematical theory of communication, *The Bell System Technical Journal*, vol. **27**, no. 3, pp. 379–423, July 1948. doi: https://doi.org/10.1002/j.1538-7305.1948.tb01338.x

Tsai D.M., Chen, Y.H. 1992. *A fast histogram-clustering approach for multi-level thresholding, Pattern Recognition Letters*, Volume **13**, Issue 4, Pages 245–252, ISSN 0167-8655, DOI: https://doi.org/10.1016/0167-8655(92)90075-B

Downloaded from http://onepetro.org/SPEADIP/proceedings-pdf/22ADIP/1-22ADIP/D012S145R004/3045811/spe-211691-ms.pdf by China University of Petroleum (East China) user on 08 July 2023

Weibel, E.R. 1979. Stereological Methods," V. **1**, p. 26 in Practical Methods for Biological Morphometry, Academic Press, Inc., London

Yen, J., Chang, F., Chang, S. 1995. A new criterion for automatic multilevel thresholding. *IEEE transactions on image processing: a publication of the IEEE Signal Processing Society*, **43**, 370–378

Downloaded from http://onepetro.org/SPEADIP/proceedings-pdf/22ADIP/1-22ADIP/D012S145R004/3045811/spe-211691-ms.pdf by China University of Petroleum (East China) user on 08 July 2023